robotics

MDPI

Article

Going Hands-free: MagnetoSuture™ for Untethered Guided Needle Penetration of Human Tissue Ex Vivo

Lamar O. Mair [1,*,†], Sagar Chowdhury [1,†], Xiaolong Liu [2], Onder Erin [2], Oleg Udalov [1], Suraj Raval [3], Benjamin Johnson [4], Sahar Jafari [1], David J. Cappelleri [4,5], Yancy Diaz-Mercado [3], Axel Krieger [2] and Irving N. Weinberg [1]

1 Weinberg Medical Physics, Inc., North Bethesda, MD 20852, USA; sagar353@gmail.com (S.C.); udalovog@gmail.com (O.U.); sahar.jafari2011@gmail.com (S.J.); inweinberg@gmail.com (I.N.W.)
2 Department of Mechanical Engineering, Johns Hopkins University, Baltimore, MD 21218, USA; xiaolong@jhu.edu (X.L.); oerin@jhu.edu (O.E.); axel@jhu.edu (A.K.)
3 Department of Mechanical Engineering, University of Maryland, College Park, MD 20742, USA; sraval@terpmail.umd.edu (S.R.); yancy@umd.edu (Y.D.-M.)
4 Multi-Scale Robotics and Automation Lab, School of Mechanical Engineering, Purdue University, West Lafayette, IN 47907, USA; bigbenvj@gmail.com (B.J.); dcappell@purdue.edu (D.J.C.)
5 Weldon School of Biomedical Engineering, Purdue University, West Lafayette, IN 47907, USA
* Correspondence: lamar.mair@gmail.com
† These authors contributed equally to this work.

Abstract: The application of force in surgical settings is typically accomplished via physical tethers to the surgical tool. While physical tethers are common and critical, some internal surgical procedures may benefit from a tetherless operation of needles, possibly reducing the number of ports in the patient or the amount of tissue damage caused by tools used to manipulate needles. Magnetic field gradients can dynamically apply kinetic forces to magnetizable objects free of such tethers, possibly enabling ultra-minimally invasive robotic surgical procedures. We demonstrate the untethered manipulation of a suture needle in vitro, exemplified by steering through narrow holes, as well as needle penetration through excised rat and human tissues. We present proof of principle manipulations for the fully untethered control of a minimally modified, standard stainless steel surgical suture needle.

Keywords: magnetic control; magnetic needle steering; magnetic surgery; needle–tissue dynamics; sutures

Citation: Mair, L.O.; Chowdhury, S.; Liu, X.; Erin, O.; Udalov, O.; Raval, S.; Johnson, B.; Jafari, S.; Cappelleri, D.J.; Diaz-Mercado, Y.; et al. Going Hands-free: MagnetoSuture™ for Untethered Guided Needle Penetration of Human Tissue Ex Vivo. *Robotics* **2021**, *10*, 129. https://doi.org/10.3390/robotics10040129

Academic Editor: Ken Masamune

Received: 14 October 2021
Accepted: 23 November 2021
Published: 1 December 2021

1. Introduction

Suturing is a longstanding, critical, and routine component of surgical procedures and wound closure. Anthropologists have recorded ancient suture methods that include wound closure by allowing ants or beetles to bite opposing sides of a wound then detaching the insect's body, leaving the mandible stitch in place and the wound closed under the compression force of the bite [1]. Modern suturing is performed via manual or robotic suture needle manipulation, with minimally invasive surgeries (MIS) performed using robotic suturing instruments achieving increasing levels of autonomy in recent years [2]. Minimally invasive surgeries (MISs) currently involve inserting miniature manipulators into a patient via a single incision [3] or a natural orifice [4]. Such procedures routinely access hard to reach tissues through laparoscopic ports of decreasing size and number. For surgeries requiring internal sutures, the procedure is commonly performed using a suture needle and an attached thread, manipulated by surgical manipulators for needle guidance. Of these, surgical manipulators for needle guidance often require the most space inside the patient and, thus, often cause tissue damage that could be avoided if needle guidance could be performed via a tetherless application of force to steer the needle. Further minimizing the invasiveness of surgical procedures remains an important goal of surgical robotics, as manipulators used for guiding needles during interventions have the potential to initiate

infections at the surgical site, result in large scars, and may cause unnecessary damage to tissues during the manipulation process [5].

Magnetic fields are safe and can be applied at significant amplitudes and a broad range of frequencies with no ill effects, thus offering a possible route for the safe manipulation of such devices. Naturally, care must be taken to ensure the environment is free of magnetic materials not involved in the surgical procedure so as to avoid the inadvertent motion of magnetic objects by the applied magnetic fields. Recently, magnetically actuated robots, ranging from sizes on the order of 10 nanometers to a centimeter, have been developed for medical applications, including drug delivery [6], biofilm removal [7], biopsy [8], ligation [9], catheter guidance [10–12], tissue penetration [13], cutting [14], shape programming [15], and needle advancing and steering [16]. At the milli- and centimeter scale, devices and manipulation platforms for performing surgical procedures are being developed which make use of different actuation methods, manipulating a broad range of functional robotic devices [17]. Specifically, recent efforts have magnetically actuated surgical tools such as organ retractors [18,19], endoscopic cameras [20–22], catheters [23,24], and drug delivery robots [25] for enabling minimally invasive procedures.

As it stands, suturing is still a "tethered" technology in which the suture needle is manipulated via mechanically contacting the needle using fingers or robotic end-effectors for physically grasping, pushing, pulling, wiggling, or twisting the suture needle. The capability to manipulate the suture needle using non-contact methods could significantly decrease the invasiveness and resulting trauma of some surgeries. This is particularly true for suturing and other needle manipulation tasks occurring inside the body. For manipulating sharp, penetrating, needle-like devices, magnetic control techniques may obviate the need for physically contacting the suture needle, further reducing the size and number of entry ports for internal surgical procedures [26]. Recently, complex schemes of drilling particles [13,27], Gauss guns [28], and magnetic hammers [29,30] have been proposed for magnetically powered tissue-penetrating robots. These elegant methods overcome the issue of providing a sufficient force to move through the dense, entangled protein matrix that makes tissue penetration difficult for magnetically actuated tools. For sutures, the optimum suture guidance instrument minimizes tissue damage, has many degrees of freedom, is capable of exerting a broad range of forces with a high force resolution, and enables high position resolution. The untethered manipulation of suture needles may one day enable ultra-minimally invasive surgeries (u-MIS) which would involve fewer incisions and remove the need for using trocars to manipulate the surgical needle.

Here, using a magnetic system similar to that used in our previous work [9,31,32], we demonstrate the manipulation of a standard suture needle with an attached suture thread using an array of up to five electromagnets. While our previous works in this field utilize a larger system with a workspace of 100 mm on a side, the system presented here fits a Petri dish only 35 mm in diameter. A second differentiating characteristic of the present system over our previous work is the addition of a fifth coil, used here for tilting the needle out of the plane of the Petri dish floor, opening possibilities towards 3D manipulations. Here, we use the fifth coil to tilt the needle out of the plane of the Petri dish so as to enable moving the needle over and under the suture thread for tying a knot. Using this smaller system, we demonstrate the ability to steer the needle around fixed structures, stitch together adjacent sections of plastic, and (separately) penetrate a segment of rat intestine and a segment of human skin ex vivo. Contributions of this paper include the first demonstration of a magnetic suture system being used to penetrate human skin ex vivo, the first demonstration showing applications to standard surgical needles without NdFeB hard magnet modifications, and the first demonstration using MagnetoSuture™ to generate an out-of-plane motion for tilting the suture needle so as to tie a rudimentary knot.

2. Materials and Methods

2.1. Manipulation System and Suture Needle Magnetization

Our manipulation system consisted of four electromagnet coils (EMs) arrayed in a plane (X–Y plane), separated by 90 degrees. Faces of opposing EMs were 40 mm apart. Each EM had an inner diameter of 22 mm, an outer diameter of 40 mm, and a length of 40 mm, having 14 layers of windings with 29 turns per winding, created using AWG 16 magnet wire. Coils were wound on 3D-printed forms composed of high-performance polyetherimide (PEI) thermoplastic (ULTEM™ 1010 resin, Stratasys Direct). Iron cores (40 mm long, 19 mm diameter) were inserted into the EMs to increase the field and gradient generated during activation. Coils were energized by PWM supplied by RoboClaw motor controllers powered by AC/DC converters (60 V, 55 A output, CUI Inc., Tualatin, OR, USA). Two dual-channel motor controllers were used for 2D manipulation, with each coil being individually addressable and bipolar. EMs were controlled by wireless remote controller (Spektrum SPMR6750 DX6), and individual coil current ranged from −20 A to 20 A. Figure 1A shows a schematic of the experimental hardware and remote controller. Figure 1B shows a photograph of the coil array and inserted Petri dish. When necessary, a fifth coil, placed above the sample Petri dish, was inserted and powered by a separate motor controller and wireless remote (not shown). The fifth coil was used for suturing acrylic sections and knot formation (Section 3.2). This fifth coil allowed for tilting the tip or tail of the needle out of the X–Y plane, significantly expanding the capabilities for experiments such as targeting out-of-plane holes or passing the needle over or under the suture thread. The coil array was partially submerged in a bath of ice water (for cooling EMs) and placed on a transmitted light stage. Thus, all experiments were backlit, with the camera collecting images from above the workspace.

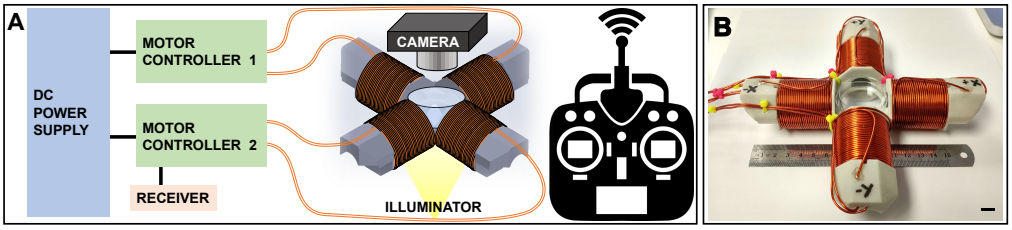

Figure 1. (**A**) Schematic of power system, motor controllers, receiver, coil array with illuminator and camera, and handheld remote controller ((**A**), right). The handheld remote controller converted the operator's movements into a radio signal and broadcast this signal to the receiver, which was previously bound to the handheld remote controller via recognition and confirmation of the remote controller's Globally Unique Identifier (GUID). (**B**) Photograph of coil array sitting on a ruler (units in centimeters). The central region of interest fit a 35 mm diameter Petri dish. Scale bar is 1 cm.

All experiments were performed using standard surgical steel suture needles (ARO-Suture E11A06N-45, AROSurgical Instruments Corporation, Newport Beach, California, USA). Needles were 0.39 mm in diameter and 11 mm long, with 3/8 circle curvature prior to straightening, and extra reverse cutting tips. Needles were swaged, with the suture filament being attached by passing through a laser drilled hole in the suture needle. Suture thread was non-absorbable black polyimide monofilament, size 6-0 (0.07 mm diameter). Needles were straightened with pliers, then magnetized by sliding the needle against a NdFeB magnet (K&J Magnetics, DX0Y0, 25.4 mm diameter, 50.8 mm length, axially magnetized, surface field of 640 mT). The suture needles were composed of 304 stainless steel, coated with a thin layer of silicone, and sterilized by electron beam irradiation. The 304 surgical stainless steel had some small remanent magnetization that persisted so long as the needle remained below the Curie temperature and was not magnetically switched due to the application of a large, opposing magnetic field. As discussed below in Section 2.3, the needle was pre-magnetized with a strong magnetic field provided by a permanent magnet prior to use. The modeling section discusses needle magnetics further.

2.2. Experimental Setup and Sample Preparation

All experiments were performed in 35 mm diameter Petri dishes with honey or dilute honey used as the fluid medium for motion. The increased viscosity of honey was used to decrease needle velocity, thereby making fine-tuned motion control of the needle easier to accomplish using the handheld remote controller. Decreased needle velocity was particularly useful in scenarios where meticulous needle positioning was required for completion of the designed task. Various experimental setups were generated for specific types of tests. These scenarios included steering the suture needle around three fixed-location hexagonal nuts, steering the needle so as to stitch together two pieces of acrylic having pre-drilled holes, and steering the needle so as to penetrate a section of tissue (rat intestine, human skin). For steering around hexagonal nuts experiments, nuts were glued to the Petri dish and the dish was filled with 100% honey. A suture needle with a shortened suture thread was maneuvered around the nuts. For stitching together plastic pieces, acrylic sections were placed side-by-side in the Petri dish (held in place by a twist tie) and a suture needle with a full suture thread attached was used. For rat tissue penetration experiments, rat intestine (BioIVT) was rinsed in saline solution, sectioned, and then secured between two aluminum tissue mounts. For human tissue penetration experiments, skin was excised from a blister on the heel and placed in the MagnetoSuture™ workspace. The heel tissue was mounted in a poly(dimethylsiloxane) (PDMS) holder that kept the tissue from being pushed out of place by the needle during the magnetic needle penetration experiment.

2.3. Modeling

Here we provide some modeling on needle magnetization as well as equations for understanding forces and torques on steel needles in magnetic fields. Additionally, we provide simulations of the magnitude of magnetic field possible using our coil array so as to provide the reader with a picture of the spatial distribution of field magnitude in the manipulation workspace when the coils were activated in various configurations (Figure 2). Our magnet geometry utilizing four (or five) coils was chosen based on the desire to have a simple system which offered easy access to the sample and was moderately portable. Here, we provide information that informs expectations regarding system geometry, workspace size, distribution of magnetic fields in the workspace, and manipulation of steel needles.

The suture needle was pre-magnetized along the needle's major axis with a strong magnetic field from a permanent magnet. We denoted the finite remanent magnetization along the axial direction of the needle as $\overrightarrow{m_{\mathrm{r}}} = \begin{bmatrix} m_{\mathrm{r}} & 0 & 0 \end{bmatrix}$ (in the needle's coordinate frame), where the first element was the axial direction along the needle's length. In addition to the remanent magnetization, there was a field-induced magnetization in the needle. It occurred due to the soft magnetic properties of the needle material. The induced magnetization could be described by the expression $\overrightarrow{m_{\mathrm{i}}} = \mu N \overrightarrow{H}$, where $\overrightarrow{H}$ is the external magnetic field acting on the needle, μ is the needle magnetic susceptibility, and N is the magnetizing factors tensor. Due to the elongated shape of the needle, the component of the N-tensor along the needle axis was much larger than the perpendicular components [33]. Therefore, generally, $\overrightarrow{m_{\mathrm{i}}}$ was not co-directed with the external field. The total magnetic moment $\overrightarrow{m_{\mathrm{t}}}$ was the sum of remanent and induced magnetizations. The ratio between these contributions depended on the external field strength and was not studied in the present work.

For our magnetic needle in the Petri dish exposed to magnetic fields and gradients, the magnetic force acting on the needle was given by:

$$\overrightarrow{F} = \nabla(\overrightarrow{m}_{\mathrm{t}} \cdot \overrightarrow{H}) = \overrightarrow{m_{\mathrm{r}}} \cdot \nabla \overrightarrow{H} + 2\mu \overrightarrow{H} N \nabla \overrightarrow{H} \quad (1)$$

and the torque was given by:

$$\overrightarrow{\tau} = \overrightarrow{m}_{\mathrm{t}} \times \overrightarrow{H} = \overrightarrow{m}_{\mathrm{r}} \times \overrightarrow{H} + \mu \overrightarrow{H} \times N \overrightarrow{H}. \quad (2)$$

Both contributions, generally, induced needle translation and rotation. The second component of the force always pulled the needle to the region with stronger magnetic field (usually toward the magnets). The first component may either pull or push the needle depending on the needle's orientation. However, in our experiments, the magnetic field gradient changed slowly in time (insufficiently fast to cause magnetization direction reversal) and the needle axis and magnetization directions followed the local magnetic field direction. Therefore, the action of this component was similar to the second one and the needle was pulled to the region with stronger field.

To demonstrate the field magnitudes and field distributions for energized electromagnets, we simulated magnetic field maps for three different configurations (Figure 2). Simulations for single-coil activation (+20 A), as well as double-coil activation with the same (+20 A, +20 A) and opposite (+20 A, −20 A) current directions, are shown in Figure 2A–C, respectively.

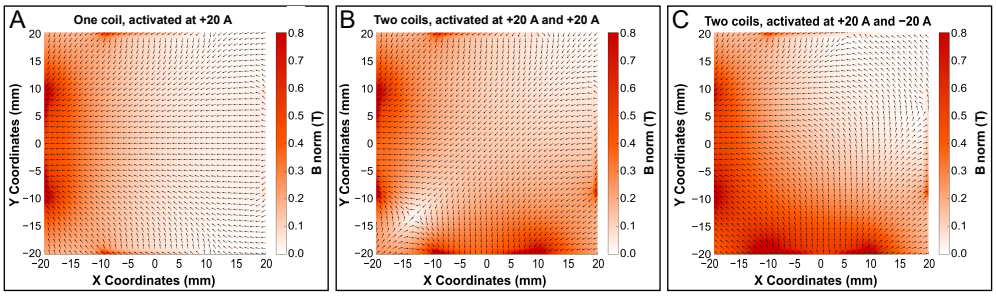

Figure 2. Simulations of the magnitude (B norm) of magnetic fields generated for various conditions, with inserted iron cores. Simulations cover a square sample area of 40 mm on a side. (**A**) Magnetic field in the case of one coil energized at +20 A. (**B**) Magnetic field in the case of two coils both energized at +20 A. (**C**) Magnetic field in the case of one coil energized at +20 A and a second adjacent coil energized at −20 A.

For all experiments, the needle was moved through a fluid with minimum viscosity of 10^{-4} Pa·s (water) and a maximum viscosity of 10 Pa·s (honey). Our steel needle experienced forces due to magnetic field gradients, fluid drag, gravity (ignored due to 2D nature of experimental setup), and friction due to needle interactions with the Petri dish surface. Understanding the Reynolds number Re of our needle in the range of fluids used was a helpful exercise in understanding and anticipating needle movement. Reynolds number, a ratio of inertial forces to viscous forces, is given by

$$Re = \frac{\rho u D}{\mu_{fluid}}, \tag{3}$$

where D is the characteristic length of the object, ρ is the fluid density, u represents the object's velocity, and μ_{fluid} denotes the dynamic viscosity of the fluid. For our needle having diameter of 0.39 mm, the needle speed needing to reach $Re = 1$ was approximately 2.3 mm/s in water and greater than 9000 mm/s in honey (dynamic viscosity of water $\mu_{water} \approx 8.9 \times 10^{-4}$ Pa·s, dynamic viscosity of honey $\mu_{honey} \approx 10^{1}$ Pa·s). As most experiments took place in honey or diluted honey, and since the velocity of the needle was in orders of magnitude less than the speed to obtain $Re = 1$ in honey, the drag forces acting on the needle could be modeled as largely in the Stokes flow regime [34]. In pure water, it is likely that we would begin to see non-Stokes flow behavior from the needle, particularly near the coils. Due to the scalability of the unitless Re number, using honey allowed us to emulate the experiments in smaller scales by keeping the same Re number, where the needle was much smaller and the medium was less viscous (i.e., water instead of honey) [35]. Therefore, studies here may demonstrate further applicability in the realm of magnetic microrobotics.

3. Results and Discussion

3.1. Manipulation around Fixed Structures

Our coil array and remote control manipulation hardware enabled us to steer the suture needle around fixed structures in a truly untethered manner. By truly untethered, we mean that the user wirelessly communicated with the motor controllers and the suture needle was manipulated via magnetic fields and gradients. In previous iterations, the MagnetoSuture™ control system used handheld controllers tethered to a logic board. Here, we present modifications that enabled wireless communication between a handheld remote controller and motor controllers. While a modest change, the protocol allowed the operator to be fully untethered from the manipulation of the magnetic suture needle. First, demonstrations performed a lemniscate pattern around two of the fixed hex nuts (Figure 3). Hex nut manipulation experiments were performed in 100% honey. In honey, the needle was steered around the hex nuts in the Petri dish and the suture thread glided easily over the hex nut structures. The purpose of the manipulation around fixed structures was to confirm that the selected hardware and remote controller provided sufficient control via user-friendly, robust, wireless communication before moving on to more challenging manipulation tasks. Video of the manipulation is included as Supplementary Information.

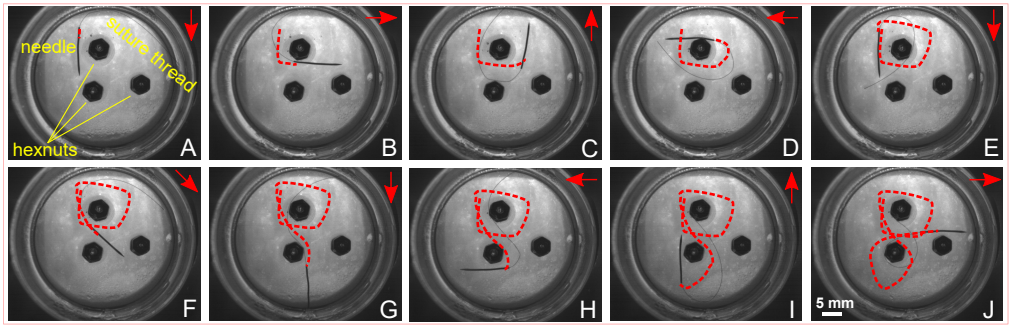

Figure 3. The suture needle was steered in a lemniscate pattern around fixed metallic nuts using handheld manual controller. (**A**) Needle, suture thread, and hex nuts (affixed to the Petri dish) are labeled. Red arrows in the upper right corners of each panel indicate the direction of increasing magnetic gradient and the corresponding pointing direction of the needle anticipated at that time during the manipulation. (**B**–**J**) Dotted red lines generally outline the path of the needle throughout the manipulation. (**J**) A lemniscate pattern was completed around two hex nuts. The manipulation took approximately 7 min. to perform. Video is included in Supplementary Information.

3.2. Suturing Acrylic Sections

Suturing pieces of tissue together was the ultimate task for the MagnetoSuture™ system. The task required repeated targeting and passage through two segments of material. The purpose of suturing acrylic sections was to determine what challenges would need to be overcome in the manually controlled magnetic manipulation of a needle with an attached suture thread for repeated passage through segments of material. Here, we modeled such a capability using clear plastic (acrylic sheets), which contained pre-drilled holes for passing the suture needle, stitching together the two pieces with the attached suture thread (Figure 4A–J). The final manipulation accomplished tying a simple overhand knot after the two segments were sewn together. Additionally, because the holes in the acrylic were above the floor of the Petri dish, a Z-axis coil was implemented to enable tilting the needle out of the X–Y plane. Tilting the needle was critical not only for aiming the needle into the pre-drilled holes (≈1.5 mm diameter), but also for allowing the needle to move over/under the suture thread for passing the needle through a loop of thread (Figure 4L), knot formation (Figure 4M), and knot tightening (Figure 4N,O). The Z-axis coil was powered via PWM controlled by a third RoboClaw motor controller receiving signals from a second remote controller operated by a second user. Using all five EMs, the suture needle passed through the pre-drilled holes repeatedly, weaving together the two pieces

as the maneuvers were completed. Figure 4 demonstrates this process, culminating in a rudimentary overhand knot being formed by passing the needle through a loop of thread and pulling the thread taught against one side of the acrylic sheet (Figure 4K–O).

Due to the low magnetization of the needle, it was challenging to provide sufficient magnetic force to overcome the friction of the suture thread being looped through the acrylic multiple times in all suture thread configurations. As shown in the accompanying Supplementary Information Video, some interventional assistance via manual thread manipulation was required (timestamps 24:48 through 25:02). EMs capable of generating stronger fields and gradients could significantly increase suturing capabilities.

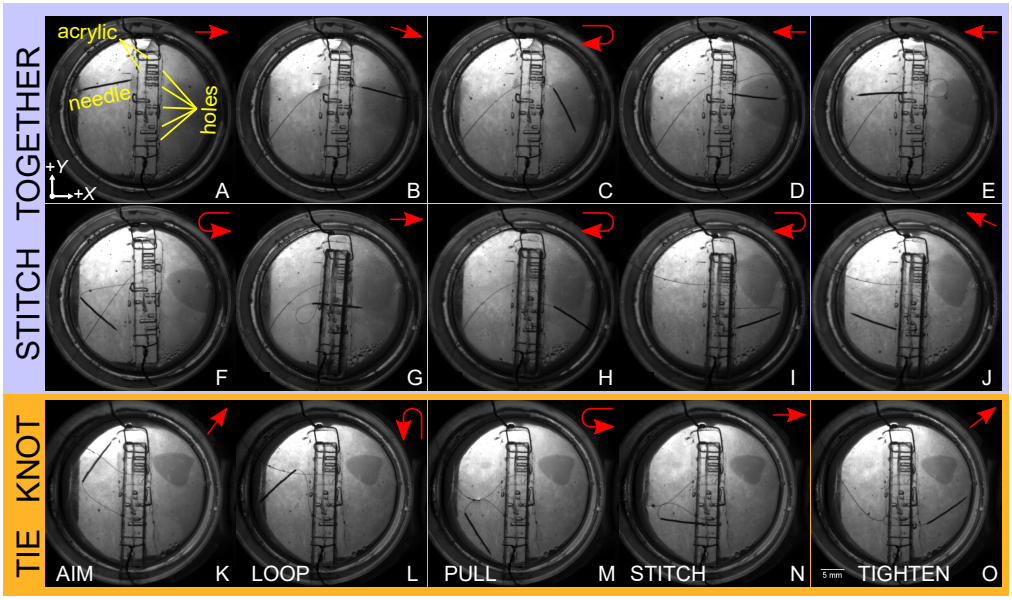

Figure 4. Stitching together two pieces of acrylic via sequential targeting and passage through pre-drilled holes. Red arrows in the upper right corner of each panel describe the maneuver being performed in terms of the pointing direction of the needle tip, as well as the direction of increasing magnetic gradient. (**A**) The needle, acrylic, and holes in acrylic are labeled. The needle began the stitching procedure, completing one passage in (**B**). The needle turned around in (**C**,**D**), then completed a second passage in (**E**). In (**F**), the needle turned around again, proceeding through a third passage in (**G**), before turning around in (**H**,**I**) and completing a fourth passage in (**J**). In (**K**) through (**O**), the needle was manipulated so as to tie a rudimentary overhand knot. First, in (**K**), the needle was aimed towards the initial starting position; then, in (**L**), the needle looped under the starting thread, returned over the starting thread, and in (**M**) began to pull the knot tight. In (**N**), the needle entered a hole in the acrylic, and in (**O**), the needle completed its final passage, tightening the knot against the acrylic sheet on the left side. A full video is available in the Supplementary Information.

3.3. Penetrating Rat Intestine

Without haptic force feedback, operators performing tetherless manipulation under magnetic guidance lack a sense of how a suture needle interacts with the tissue. The purpose of penetrating rat intestine was to determine if any unique dynamics or manipulations would be required for the penetration of ex vivo tissue using the magnetic guidance of a standard suture needle. A segment of cleaned, rinsed rat intestine was mounted against the floor of the Petri dish and the needle was brought into contact with the intestine and simultaneously pulled along the +X direction so as to first pierce the tissue (Figure 5). Subsequently, the needle was oscillated in the +Y/−Y directions so as to enable the needle to move through the tissue. Figure 5A shows the experimental setup, with rat intestine pinned to the floor of the dish using aluminum holders.

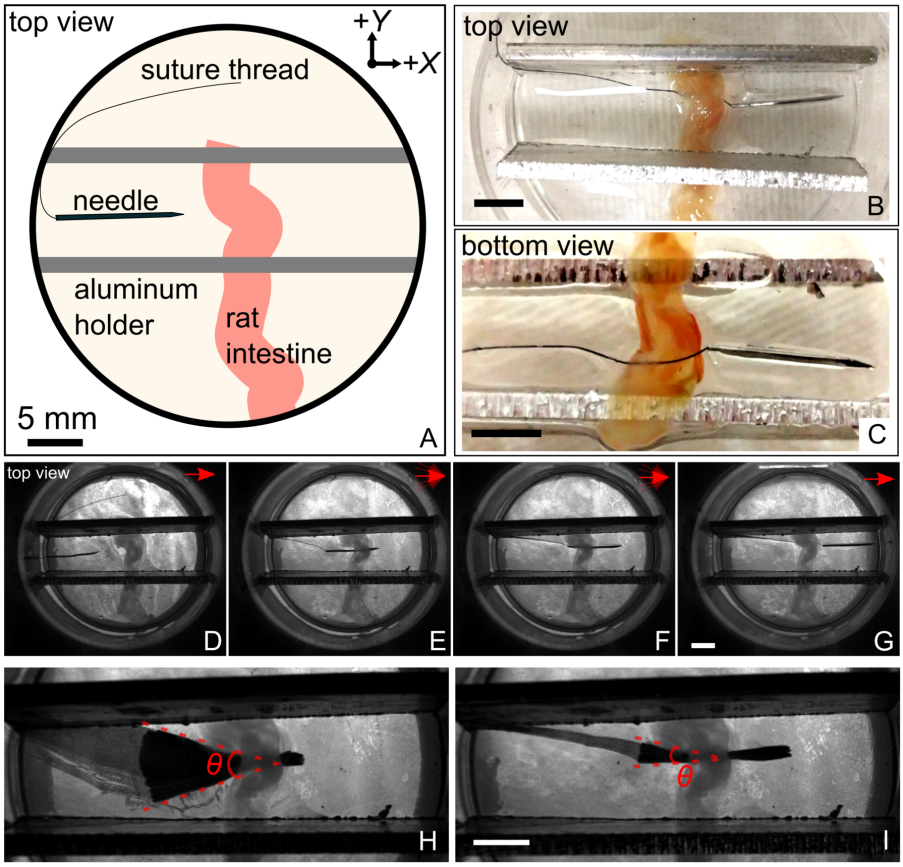

Figure 5. Figure (**A**) shows schematic of rat intestine holder, needle and shortened thread, and rat intestine positioned in Petri dish. (**B**) Top view of the rat intestine after penetration procedure. (**C**) Bottom view through the Petri dish of the rat intestine after penetration. Suture thread partially obscured as it passed through tissue. (**D**–**G**) Sequential penetration of the rat intestine under transmitted light. Red arrows in the upper right corner of each panel describe the maneuver performed in the panel in terms of the pointing direction of the needle. The needle was first pulled towards the right (**D**), then pulled through the intestine using oscillating torques (+/−Y direction) in combination with a gradient (**E**,**F**), and, finally, was free of the intestine tissue (**G**) . Red arrows in (**E**,**F**) depict the oscillations imposed on the needle via lateral magnetic fields. (**H**) Minimum intensity projection showing the swept angle θ of the needle from time 0:39 through to time 2:29, as the needle tip first penetrated the rat intestine and was oscillated along the Y-axis. (**I**) Minimum intensity projection from time 2:34 through to time 2:46 showing that, as the needle penetrated the intestine, θ diminished significantly, from $\approx 34^\circ$ initially to $\approx 15^\circ$ after the needle was embedded in the tissue, making similar magnetic fields insufficient for large θ deviations. The penetration took approximately 5 min. to perform. All scale bars are 5 mm. Video is included in Supplementary Information.

The setup allowed for the needle to contact and pierce the rat intestine without immediately going under the tissue sample. Figure 5B,C shows the top-down and bottom-up images, respectively, of the rat intestine after penetration.

The video, included as Supplementary Information, shows the needle moved into contact with the intestine, piercing the intestine, and pulled without lateral (+Y/−Y) oscillations for 20 s with little progression through the intestine. A slight mechanical deformation of the tissue was observed. Once the tip of the needle was partially lodged into the intestine and penetrative progress had essentially stalled, oscillations were induced via the activation of the Y-axis coils, generating a yaw-style motion of the needle. Torque transferred to the needle resulted in needle oscillations centered at the location where the needle was most ensnared in the tissue. Figure 5D,E shows the tissue penetration process, with the needle oscillated in the direction perpendicular to the gradient pulling

direction during penetration. During the early needle–tissue interaction period, while the suture needle was less than 20% of the way through the intestine, magnetic fields in the Y-axis swept the tail of the needle through the $\theta \approx 34^{\circ}$ range of deflection (Figure 5H). Large oscillation angles were possible because only the tip of the needle was mechanically ensnared by the tissue. Once the needle was halfway lodged into the intestine, Y-axis fields of equivalent field strength induced smaller oscillations of the $\theta \approx 15^{\circ}$ range of deflection (Figure 5I). Control mechanisms were able to position needles and apply force for penetration despite the slippery surfaces of rat intestine, possibly due to the very sharp tip of the suture needle.

3.4. Penetrating Human Tissue

The final objective of a MagnetoSuture™ system would be sequential penetration of human skin. Our purpose here was to demonstrate, for the first time, the magnetically guided penetration of human tissue ex vivo using a standard suture needle with an attached thread. Here, we demonstrated the ability to penetrate a single layer of excised human heel tissue (Figure 6). Figure 6A shows a schematic of the experiment, and Figure 6B shows a photograph of the sample, holders, skin, needle, and thread after the needle had passed through the skin twice. Figure 6C–J show stills from the skin penetration process. As in the case of the rat intestine, the process began by engaging the needle with the skin and initiating a back and forth motion of the needle. Because the needle had a low overall magnetization and the magnetic gradients generated were relatively small, there was insufficient force to induce a smooth penetration of the needle through the tissue. As was the case in the rat intestine experiments, the needle was first moved into contact with the tissue. As in the rat intestine experiments, the initial penetration was the most time-consuming aspect of the procedure, with the needle velocity increasing substantially after the initial hole formation. Once the initial penetration was partially accomplished, the needle was magnetically wiggled side to side so as to enable penetration into and passage through the tissue (Figure 6E). After repeated back and forth motions (along the Y-axis) with a combination of a magnetic gradient pulling the needle (in the +X direction) into the tissue, penetration was accomplished (Figure 6F). Turning the needle around and aiming it at a site near the original penetration, we successfully guided the needle back through the tissue at a different location; thus, demonstrating proof of principle for the repeated MagnetoSuture™ penetration of human skin (Figure 6B,J). Importantly, the initial penetration of the tissue required small oscillation angles $\theta \approx 32^{\circ}$, as shown in Figure 6K. Larger oscillation angles generated prior to the initial penetration resulted in slippage between the tissue and the needle tip, making penetration impossible. Once the tip of the needle had penetrated the tissue, larger oscillation angles of $\theta \approx 93^{\circ}$ were possible without dislodging the needle from the tissue, as shown in Figure 6L. This switch from small initial oscillations to larger final oscillations differed from the case of the rat intestine penetration possibly due to differences in tissue thickness, surface properties, or elastic modulus. The skin being a comparatively thin tissue sample allowed for larger deviations after penetration as compared with the thicker intestine tissue.

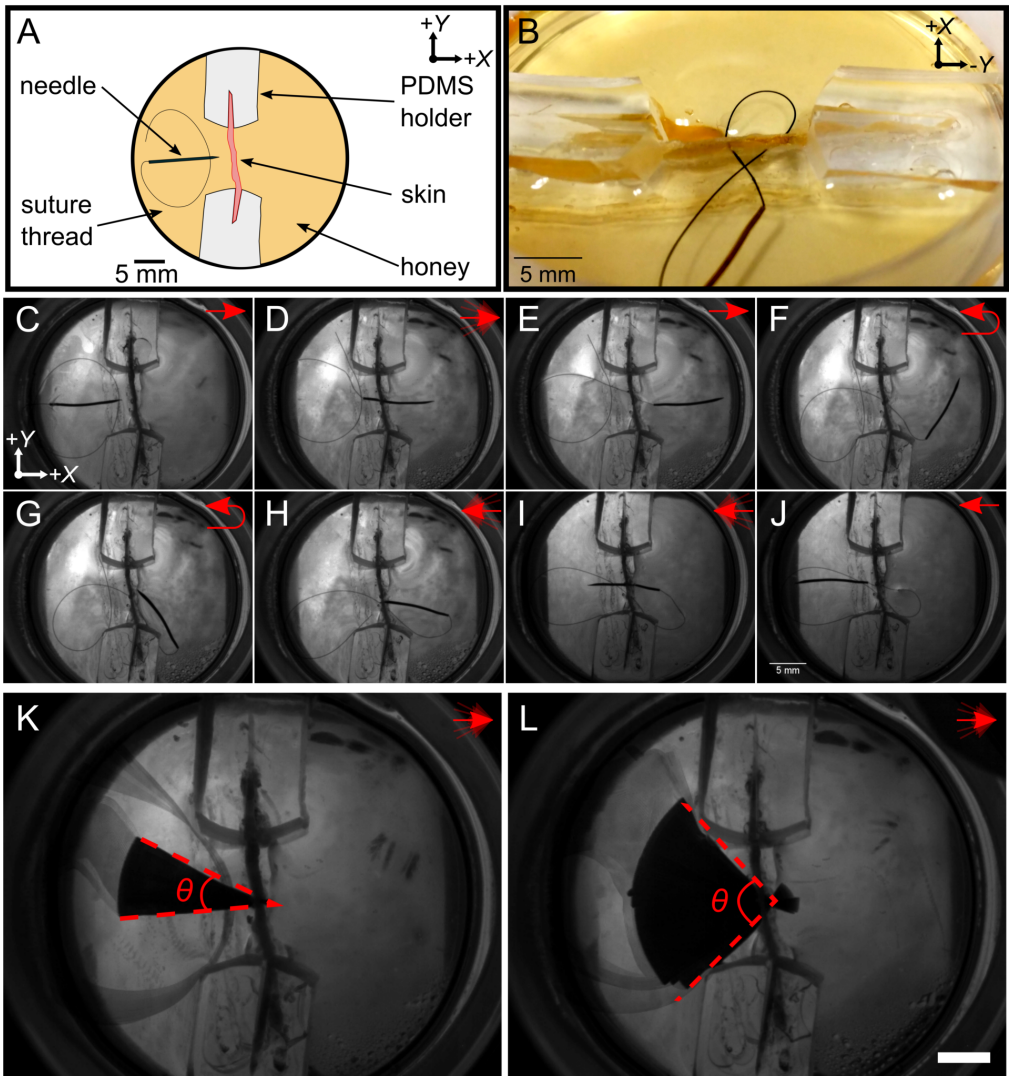

Figure 6. (**A**) Schematic of skin holder and experiment; (**B**) photograph of skin after double penetration using suture needle and thread. (**C**) through (**J**) show the sequential penetration of the human heel skin with the gradients first pulling in the +X direction (**C**–**E**), then turning around (**F**,**G**), and pulling in the −X direction (**H**–**J**). Red arrows in the upper right corner of each panel describe the maneuver performed in the panel in terms of the pointing direction of the needle. (**K**) shows a minimum intensity projection, depicting the oscillation angle θ used during initial needle–tissue interactions. Initial oscillations of $\theta \approx 32^\circ$ were purposefully small, as the needle could be seen to slip in respect to the tissue surface when larger oscillations were applied prior to tip penetration. Here, small oscillation angle ensured that the penetration point was retained during changing needle angles. (**L**) shows a minimum intensity projection, depicting the oscillation angle θ once the tip had penetrated the layer of skin and tip-surface slippage was no longer a concern. Once the tip of the needle was securely through the tissue, larger oscillations of $\theta \approx 93^\circ$ allowed for more rapid progression of the remainder of the needle through the puncture. Scale bar in (**K**,**L**) is 10 mm. Red arrows in (**D**,**H**,**I**,**K**,**L**) depict the oscillations imposed on the needle via lateral magnetic fields. Video is included in Supplementary Information.

4. Future Work

We presented proof of principle for using a standard suture needle, free of NdFeB magnetic materials, to perform human skin penetration under magnetic guidance. There were several limitations of the system, including, but not limited to, the small size of the workspace, low magnetic fields, lack of force feedback, lack of closed-loop control, and long experimental times for accomplishing manipulation and tissue penetration tasks. Overall

improvements to the system could be performed by increasing the current in the coils and adding turns to the coils. Furthermore, significant improvements in speed and control performance could be possible with increased user expertise and experience in needle manipulation obtained via practice with the tool. Adding computer vision and computer-aided control techniques would also improve control and reduce task completion times.

4.1. Needles in the MagnetoSuture™ System

The needle design, needle magnetization, needle sharpness, and actuation strategy all play an important role in tissue penetration. These factors all affect how easy it is for any given needle to pierce tissue, and what magnetic fields or field pulses are required to generate sufficient force for steering and penetration. Increasing the force on needles may be accomplished by increasing the magnetization embodied by the needle, either by adding more magnetic material (such as NdFeB) or making the needle larger. We previously described MagnetoSuture™ efforts using magnetic gradient pulling applied to three different needles. Our initial work used a sharpened cylindrical NdFeB magnet ≈25.4 mm long and 1.6 mm in diameter [9,31]. Improving upon that simple design, Pryor et al. manipulated a 22 G hypodermic stainless steel needle (0.413 mm inner diameter, 0.7176 mm outer diameter, 23.5 mm length) with embedded NdFeB magnets (0.3 mm diameter, 0.5 mm length, 42 inserted magnets, axially magnetized), demonstrating the ability to find and track the needle in highly occluded environments [32]. Increasing the force on needles may also be accomplished by switching from magnetic pulling forces to magnetically-induced impact-based forces. Improvements over the gradient pulling technique were determined by Leclerc et al. [29], as well as Erin et al. [30], via the demonstration of a magnetic hammer composed of a hypodermic needle tip (14 G) attached to a hollow plastic tube having movable internal NdFeB magnets. In both cases, the hammering mechanism was used to demonstrate tissue penetration. In the case of Erin et al., the magnetic hammer yielded a 22.7-fold increase in force applied to the needle as compared with gradient pulling forces.

While previously published needles were able to penetrate tissues as shown here, those needles all consisted of some hard magnetic material (NdFeB) incorporated into the needle architecture. Standard suture needles of surgical stainless steel are ubiquitous, inexpensive, easy to obtain, commonly used across multiple medical fields, come in a variety of shapes and sizes, and can be magnetically manipulated without any further modification to the needle. As discussed in Section 2.3, these surgical stainless steel needles have both remanent and induced magnetization. As these needles are commonly used, future work detailing how induced needle magnetization responds to specific applied magnetic fields would enable an increasingly accurate control of such needles in magnetic manipulation systems. Here, we demonstrated that solid surgical 304 stainless steel can be used to accomplish basic tissue penetration procedures using only magnetic forces and torques. The only modification to the needle was straightening the needle and stroking the needle against a permanent magnet to increase the needle's remanent magnetization. Demonstrating tissue penetration with standard suture needles absent of NdFeB components is an important step in demonstrating the proof of principle for magnetic suturing protocols.

While we demonstrated the penetration of skin, tissues in the body span a wide range of stiffnesses. Elastic moduli of tissues and biopolymers in the body range from 11 Pa (intestinal mucus) to 20 GPa (cortical bone), with brain typically having ∼1 kPa and skin having an elastic modulus of ∼100 MPa [36]. Future work will explore penetration through various tissues.

Many common procedures rely on curved suture needles. Our use of straight needles in the present work was clearly a limitation, as we were uncertain how a curved needle would move under such forces. However, curved needles maintain an overall remanent magnetization and magnetization vector. In the presence of a magnetic field, it would be expected that this overall remanent magnetization would cause the needle to align its overall magnetization vector with the applied field, granted the magnetic field induces torque sufficient for needle rotation, given the surrounding material.

4.2. The Significance of Lateral Magnetic Fields for Enhancing Translation through Biomaterials

Previous experiments employing oscillations [37] and rotating fields [38,39] to enhance the transport of microscale and nanoscale particles through biologically relevant gels and tissues have demonstrated the advantage of combining gradient pulling with time-varying fields oriented perpendicular to the gradient. Needle rotation has been demonstrated to improve targeting and reduce needle placement errors by as much as 17% [40]. Here, we demonstrated that perpendicular, time-varying fields can be implemented to improve penetration for centimeter-scale needles. Future directions may take advantage of these time-varying fields, possibly employing combined pulling sutures with screw-shaped surgical segments that can also drill through tissues, as has been demonstrated by Rahmer et al. [13]. Here, standard surgical needles composed of surgical steel were able to penetrate rat and human tissue using magnets placed close to the sample region. However, other methods such as the previously discussed magnetic hammering methods [29,30] which can significantly increase the force applied to the tip of the needle may be required to enable a long-range, clinical scale application of these robotic technologies or manipulation in larger workspaces. Additionally, imaging the needle during manipulation is a critical challenge and future efforts aim to perform suturing tasks in occluded environments under guidance from ultrasound or endoscopic imaging techniques.

4.3. Magnetic Manipulation Lacks Inherent Haptic Force Feedback

A major disadvantage of untethered surgical operations is that force feedback to the surgeon's fingers and hands is not inherent. This is a common issue in magnetic manipulation and may pose a serious challenge to the concept of magnetically guided surgical intervention. Our ex vivo manipulations were plagued with issues of the needle overshooting its target location immediately after a tissue penetration event. This was due to the needle localization having no accompanying local viscosity or local motion resistance information transferred back to the operator, as well as a slow operator response time. Previous demonstrations of magnetic needle steering and magnetic needle guidance have largely focused on mechanically uniform needle environments in which the viscosity was uniform or varied only slightly [16,24]. Our experiments included solids, liquids, and needle passage from liquids, through solids, and back into liquids. Our work showcased how, in mechanically heterogeneous environments, hand-guided magnetic manipulation without haptic force feedback fails to capture a critical aspect of successful surgical procedures taking place in such heterogeneous environments. Future work in the field would benefit from control methods using image-based force feedback into haptic devices capable of providing variable resistance to the remote user interface/hardware being used by the operator.

Based on our experiences so far, the lack of haptic feedback on the needle that is typically available for standard suturing operations performed by a surgeon may lead to safety issues. Additionally, the nonlinear magnetic field distribution nature for electromagnets may result in snapping and unwanted extreme force exertion on the magnetic needles. To prevent such a complexity, and to further advance the performance of magnetic suturing, a closed-loop feedback control algorithm should be implemented. This algorithm should also take the soft-magnetic property of the needle into account, such that computations for the magnetic pulling forces are accurate. With proper localization, path planning, and control algorithms, these magnetic suture needles may one day provide an alternative to routine suturing operations.

5. Conclusions

Here, we demonstrated the manipulation of standard steel suture needles using magnetic forces, showing the ability to stitch together pieces of clear plastic, tie knots, and penetrate human tissue ex vivo. Future work aims to scale the capabilities up to larger sizes, enable larger magnetic forces over larger distances, and increase the complexity of possible field shapes and configurations generated by the system.

Supplementary Materials: The following Supplementary Information Videos are available online at https://www.mdpi.com/article/10.3390/robotics10040129/s1.

Author Contributions: Conceptualization: L.O.M., S.C. and I.N.W.; Formal analysis: L.O.M., S.C., X.L., O.E. and O.U.; Funding acquisition: L.O.M., S.C., A.K. and I.N.W.; Investigation: L.O.M., S.C., X.L. and O.U.; Methodology: L.O.M., S.C., X.L. and I.N.W.; Project administration: L.O.M., S.C. and I.N.W.; Resources: L.O.M. and I.N.W.; Supervision: L.O.M., S.C. and I.N.W.; Validation: L.O.M. and S.C.; Visualization: L.O.M., S.C. and X.L.; Writing—original draft: L.O.M., S.C., X.L., O.E. and O.U.; Writing—review and editing: L.O.M., S.C., X.L., O.E., O.U., S.R., B.J., S.J., D.J.C., Y.D.-M., A.K. and I.N.W. All authors have read and agreed to the published version of the manuscript.

Funding: This paper was supported by the University of Maryland Medical Device Development Fund (MDDF) and the National Institute of Biomedical Imaging and Bioengineering (NIBIB) of the National Institutes of Health under award number R01EB020610. The content is solely the responsibility of the authors and does not necessarily represent the official views of the National Institutes of Health.

Data Availability Statement: Not applicable.

Conflicts of Interest: The authors declare no conflict of interest. The funders had no role in the design of the study; in the collection, analyses, or interpretation of data; in the writing of the manuscript, or in the decision to publish the results.

References

1. Gudger, E.W. Stitching Wounds with the Mandibles of Ants and Beetles. A Minor Contribution to the History of Surgery. *JAMA* **1925**, *84*, 1861–1864.
2. Shademan, A.; Decker, R.S.; Opfermann, J.D.; Leonard, S.; Krieger, A.; Kim, P.C.W. Supervised autonomous robotic soft tissue surgery. *Sci. Transl. Med.* **2016**, *8*, 337ra64. [CrossRef]
3. Antoniou, S.A.; Pointner, R.; Granderath, F.A. Single-incision laparoscopic cholecystectomy: A systematic review. *Surg. Endos.* **2011**, *25*, 367–377. [CrossRef] [PubMed]
4. Chamberlain, R.S.; Sakpal, S.V. A Comprehensive review of single-incision laparoscopic surgery (SILS) and natural orifice transluminal endoscopic surgery (NOTES) techniques for cholecystectomy. *J. Gastrointest. Surg.* **2009**, *13*, 1733–1740. [CrossRef]
5. Gandaglia, G.; Ghani, K.R.; Sood, A.; Meyers, J.R.; Sammon, J.D.; Schmid, M.; Varda, B.; Briganti, A.; Montorsi, F.; Sun, M.; et al. Effect of Minimally Invasive Surgery on the Risk for Surgical Site Infections: Results From the National Surgical Quality Improvement Program (NSQIP) Database. *JAMA Surg.* **2014**, *149*, 1039–1044. [CrossRef]
6. Zhang, H.; Li, Z.; Gao, C.; Fan, X.; Pang, Y.; Li, T.; Wu, Z.; Xie, H.; He, Q. Dual-responsive biohybrid neutrobots for active target delivery. *Sci. Robot.* **2021**, *6*, 9519eaaz. [CrossRef]
7. Mair, L.O.; Nacev, A.; Hilaman, R.; Stepanov, P.Y.; Chowdhury, S.; Jafari, S.; Karlsson, A.J.; Shirtliff, M.E.; Shapiro, B.; Weinberg, I.N. Biofilm disruption with rotating microrods enhances antimicrobial efficacy. *J. Magn. Magn. Mater.* **2017**, *427*, 81–84. [CrossRef]
8. Gultepe, E.; Randhawa, J.S.; Kadam, S.; Yamanaka, S.; Selaru, F.M.; Shin, E.J.; Kalloo, A.N.; Gracias, D.H. Biopsy with Thermally-Responsive Untethered Microtools. *Adv. Mater.* **2013**, *25*, 514–519. [CrossRef]
9. Mair, L.O.; Liu, X.; Dandamudi, B.; Jain, K.; Chowdhury, S.; Weed, J.; Diaz-Mercado, Y.; Weinberg, I.N.; Krieger, A. MagnetoSuture: Tetherless Manipulation of Suture Needles. *IEEE Trans. Med. Robot. Bionics* **2020**, *2*, 206–215. [CrossRef]
10. Faddis, M.N.; Blume, W.; Finney, J.; Hall, A.; Rauch, J.; Sell, J.; Bae, K.T.; Talcott, M.; Lindsay, B. Novel, Magnetically Guided Catheter for Endocardial Mapping and Radiofrequency Catheter Ablation. *Circulation* **2002**, *106*, 2980–2985. [CrossRef] [PubMed]
11. Ernst, S.; Ouyang, F.; Linder, C. Initial experience with remote catheter ablation using a novel magnetic navigation system. Magnetic remote catheter ablation. *ACC Curr. J. Rev.* **2004**, *13*, 51–52. [CrossRef]
12. Chautems, C.; Tonazzini, A.; Floreano, D.; Nelson, B.J. A variable stiffness catheter controlled with an external magnetic field. *IEEE Int. Conf. Intell. Robots Sys. (IROS)* **2017**, *2017*, 181–186. [CrossRef]
13. Rahmer, J.; Stehning, C.; Gleich, B. Remote Magnetic Actuation Using a Clinical Scale System. *PLoS ONE* **2018**, *3*, e0193546. [CrossRef] [PubMed]
14. Onaizah, O.; Diller, E. Tetherless mobile micro-surgical scissors using magnetic actuation. *IEEE Int. Conf. Robot. Autom. (ICRA)* **2019**, *2019*, 894–899. [CrossRef]
15. Lum, G.Z.; Ye, Z.; Dong, X.; Marvi, H.; Erin, O.; Hu, W.; Sitti, M. Shape-programmable magnetic soft matter. *Proc. Natl. Acad. Sci. USA* **2016**, *113*, E6007–E6015. [CrossRef]
16. Ilami, M.; Ahmed, R.J.; Petras, A.; Beigzadeh, B.; Marvi, H. Magnetic Needle Steering in Soft Phantom Tissue. *Sci. Rep.* **2020**, *10*, 2500. [CrossRef]
17. Abbott, J.J.; Diller, E.; Petruska, A.J. Magnetic methods in robotics. *Annu. Rev. Control* **2020**, *3*, 57–90. [CrossRef]
18. Rivas, H.; Robles, I.; Riquelme, F.; Vivanco, M.; Jiménez, J.; Marinkovic, B.; Uribe, M. Magnetic surgery: results from first prospective clinical trial in 50 patients. *Ann. Surg.* **2018**, *267*, 88. [CrossRef]

19. Garbin, N.; Di Natali, C.; Buzzi, J.; De Momi, E.; Valdastri, P. Laparoscopic tissue retractor based on local magnetic actuation. *J. Med. Devices* **2015**, *9*, 011005. [CrossRef]
20. Simi, M.; Silvestri, M.; Cavallotti, C.; Vatteroni, M.; Valdastri, P.; Menciassi, A.; Dario, P. Magnetically activated stereoscopic vision system for laparoendoscopic single-site surgery. *IEEE ASME Trans. Mechatron.* **2012**, *18*, 1140–1151. [CrossRef]
21. Liu, X.; Mancini, G.J.; Tan, J. Design of a unified active locomotion mechanism for a capsule-shaped laparoscopic camera system. *IEEE Int. Conf. Robot. Autom. (ICRA)* **2014**, *2014*, 2449–2456. [CrossRef]
22. Liu, X.; Mancini, G.J.; Guan, Y.; Tan, J. Design of a magnetic actuated fully insertable robotic camera system for single-incision laparoscopic surgery. *IEEE ASME Trans. Mechatron.* **2015**, *21*, 1966–1976. [CrossRef]
23. Muller, L.; Saeed, M.; Wilson, M.W.; Hetts, S.W. Remote control catheter navigation: options for guidance under MRI. *J. Cardiovasc. Magn. Reson.* **2012**, *14*, 1–9. [CrossRef] [PubMed]
24. Petruska, A.J.; Ruetz, F.; Hong, A.; Regli, L.; Sürücü, O.; Zemmar, A.; Nelson, B.J. Magnetic needle guidance for neurosurgery: Initial design and proof of concept. *IEEE Int. Conf. Robot. Autom. (ICRA)* **2016**, *2016*, 4392–4397. [CrossRef]
25. Sitti, M.; Ceylan, H.; Hu, W.; Giltinan, J.; Turan, M.; Yim, S.; Diller, E. Biomedical Applications of Untethered Mobile Milli/Microrobots. *Proc. IEEE* **2015**, *103*, 205–224. [CrossRef]
26. Leong, F.; Garbin, N.; Di Natali, C.; Mohammadi, A.; Thiruchelvam, D.; Oetomo, D.; Valdastri, P. Magnetic surgical instruments for robotic abdominal surgery. *IEEE Rev. Biomed. Eng.* **2016**, *9*, 66–78. [CrossRef]
27. Ishiyama, K.; Sendoh, M.; Yamazaki, A.; Arai, K. Swimming micro-machine driven by magnetic torque. *Sens. Actuator A Phys.* **2001**, *91*, 141–144. [CrossRef]
28. Becker, A.T.; Felfoul, O.; Dupont, P.E. Toward Tissue Penetration by MRI-powered Millirobots Using a Self-Assembled Gauss Gun. *IEEE Int. Conf. Robot. Autom. (ICRA)* **2015**, *2015*, 1184–1189. [CrossRef]
29. Leclerc, J.; Ramakrishnan, A.; Tsekos, N.V.; Becker, A.T. Magnetic Hammer Actuation for Tissue Penetration Using a Millirobot. *IEEE Robot. Autom. Lett.* **2018**, *3*, 403–410. [CrossRef]
30. Erin, O.; Liu, X.; Ge, J.; Mair, L.; Barnoy, Y.; Diaz-Mercado, Y.; Krieger, A. Overcoming the Force Limitations of Magnetic Robotic Surgery: Impact-based Tetherless Suturing. *arXiv* **2021**, arXiv:abs/2107.01504.
31. Fan, M.; Liu, X.; Jain, K.; Lerner, D.; Mair, L.; Weinberg, I.; Diaz-Mercado, Y.; Krieger, A. Towards Autonomous Control of Magnetic Suture Needles. In Proceedings of the 2020 IEEE/RSJ International Conference on Intelligent Robots and Systems (IROS), Las Vegas, NV, USA, 24 October–24 January 2020; pp. 2935–2942. [CrossRef]
32. Pryor, W.; Barnoy, Y.; Raval, S.; Liu, X.; Mair, L.; Lerner, D.; Erin, O.; Hager, G.D.; Diaz-Mercado, Y.; Krieger, A. Localization and Control of Magnetic Suture Needles in Cluttered Surgical Site with Blood and Tissue. *arXiv* **2021**, arXiv:abs/2105.09481.
33. Osborn, J.A. Demagnetizing Factors of the General Ellipsoid. *Phys. Rev.* **1945**, *67*, 351–357. [CrossRef]
34. Johnson, R.E. An improved slender-body theory for Stokes flow. *J. Fluid Mech.* **1980**, *99*, 411–431. [CrossRef]
35. Qiu, T.; Gibbs, J.G.; Schamel, D.; Mark, A.G.; Choudhury, U.; Fischer, P. From Nanohelices to Magnetically Actuated Microdrills: A Universal Platform for Some of the Smallest Untethered Microrobotic Systems for Low Reynolds Number and Biological Environments. In *Workshop at the IEEE International Conference on Robotics and Automation*; Springer: Berlin, Germany, 2013; pp. 53–65. [CrossRef]
36. Guimaraes, C.F.; Gasperini, L.; Marques, A.P.; Reis, R.L. The stiffness of living tissues and its implications for tissue engineering. *Nat. Rev. Mater.* **2020**, *5*, 351–370. [CrossRef]
37. MacDonald, C.; Friedman, G.; Alamia, J.; Kenneth, B.; Polyak, B. Time-varied magnetic field enhances transport of magnetic nanoparticles in viscous gel. *Nanomedicine* **2010**, *5*, 65–76. [CrossRef] [PubMed]
38. Soheilian, R.; Choi, Y.S.; David, A.E.; Abdi, H.; Maloney, C.E.; Erb, R.M. Toward Accumulation of Magnetic Nanoparticles into Tissues of Small Porosity. *Langmuir* **2015**, *31*, 8267–8274. [CrossRef] [PubMed]
39. Jafari, S.; Mair, L.O.; Weinberg, I.N.; Baker-McKee, J.; Hale, O.; Watson-Daniels, J.; English, B.; Stepanov, P.Y.; Ropp, C.; Atoyebi, O.F.; et al. Magnetic drilling enhances intra-nasal transport of particles into rodent brain. *J. Magn. Magn. Mater.* **2019**, *469*, 302–305. [CrossRef]
40. Badaan, S.; Petrisor, D.; Kim, C.; Mozer, P.; Mazilu, D.; Gruionu, L.; Patriciu, A.; Cleary, K.; Stoianovici, D. Does needle rotation improve lesion targeting? *Int. J. Med. Robot. Comput. Assist. Surg.* **2011**, *7*, 138–147. [CrossRef]